Demonstration of high-performance, sub-micron chalcogenide glass photonic devices by thermal nanoimprint

Yi Zou[a], Loise Moreel[a], Jie Zhou[a], Danning Zhang[a], Hongtao Lin[a], Lan Li[a], Qingyang Du[a], Juejun Hu[a*], Sylvain Danto[b], Kathleen Richardson[b], J. David Musgraves[c], Kevin D. Dobson[d], Robert Birkmire[d]

[a] Department of Materials Science & Engineering, University of Delaware; Newark, Delaware USA 19716 [b] The College of Optics & Photonics, University of Central Florida, Orlando, Florida USA, 32816. [c] IRradiance Glass, Inc. Orlando, Florida USA, 32816. [d] Institute of Energy Conversion, University of Delaware, Newark, Delaware USA, 19716,

ABSTRACT

High-index-contrast optical devices form the backbone of densely integrated photonic circuits. While these devices are traditionally fabricated using lithography and etching, their performance is often limited by defects and sidewall roughness arising from fabrication imperfections. This paper reports a versatile, roll-to-roll and backend compatible technique for the fabrication of high-performance, high-index-contrast photonic structures in composition-engineered chalcogenide glass (ChG) thin films. Thin film ChG have emerged as important materials for photonic applications due to their high refractive index, excellent transparency in the infrared and large Kerr non-linearity. Both thermally evaporated and solution processed As-Se thin films are successfully employed to imprint waveguides and micro-ring resonators with high replicability and low surface roughness (0.9 nm). The micro-ring resonators exhibit an ultra-high quality-factor of 4×10^5 near 1550 nm wavelength, which represents the highest value reported in ChG micro-ring resonators. Furthermore, sub-micron nanoimprint of ChG films on non-planar plastic substrates is demonstrated, which establishes the method as a facile route for monolithic fabrication of high-index-contrast devices on a wide array of unconventional substrates.

Keywords: Chalcogenide glass, thermal nanoimprint, high-index-contrast, flexible photonics,

*hujuejun@udel.edu; phone: 302-831-2062; fax: 302-831-2062; mseg.udel.edu/

1. INTRODUCTION

High-refractive-index-contrast (HIC) waveguides and resonators allow tight bending structures and small device footprint due to strong confinement of light. Besides their well-known applications for telecommunications, HIC waveguides and resonators are essential to a number of photonic devices, such as on-chip light sources [1] nonlinear optical devices [2] and photonic sensors [3]. Despite these advantages, sidewall roughness inevitably induced by standard photolithography and dry plasma etching results in large scattering losses [4]. Since scattering loss scales with the square of index contrast [4, 5], such loss mechanisms become significant and can severely limit the performance of HIC photonic devices [5]. In order to obtain smooth device surface finish, fine-line lithography tools such as Deep-UV lithography and electron beam lithography are usually considered a must for the fabrication of low-loss HIC devices. In addition, a number of methods were applied to different material systems to smooth the device surface and enhance the optical performance. The examples include oxidation smoothing [6], post-fabrication wet etching [7], hydrogen annealing in Si/SiO_2 systems [8], laser-reformation [9], as well as thermal reflow of polymer [10] and glass materials.[11] However, most of these methods involve high temperature and multiple processing steps, which pose a challenge on device integration.

In this paper, we present the fabrication of low-loss HIC photonic devices with sub-micron dimensions by thermal nanoimprint and simple UV contact lithography. Nanoimprint lithography is an emerging technology that promises high resolution for micro- and nano-scale structure fabrication [12-14]. Additionally, it demonstrates advantages such as low cost, high throughput, and compatibility with roll-to-roll processing [15-17]. Different from traditional lithographic techniques, nanoimprint lithography is based on the mechanical molding of materials, which pose additional requirements for the imprinted materials. Specifically, the materials should be deformable under applied pressure and at the imprint processing temperature [18]. Given this requirement, conventional crystalline semiconductor materials, for example silicon, are not suitable to be used as imprinting resist materials. Several groups have demonstrated patterning polymer photonic devices by imprint methods [19-24], but they lack the aforementioned HIC-device advantages. Chalcogenide glasses (ChG), on the other hand, have suitable softening characteristics due to their amorphous nature [25]. Furthermore ChG are ideal candidates for various applications in photonic systems because of their wide transparency window from the visible to mid-IR region [26, 27], high optical nonlinearities [28, 29], high refractive indices [30, 31], photosensitivity [32, 33], and large photothermal figure-of-merit [34, 35]. The novelty of our approach lies in two aspects: firstly, we take the advantage of the low deposition temperature and amorphous nature of high-refractive-index ChG alloys to enable monolithic fabrication of HIC photonic devices on a variety of substrate materials [36, 37]. Thanks to the low processing temperature (< 50 ºC) and the demonstrated direct patterning capability on plastic substrates, our approach can potentially be compatible with CMOS backend integration as well as roll-to-roll processing. Secondly, we synergistically combined thermal reflow modification of resist pre-forms and single-step nanoimprint to create sub-micron, single-mode HIC photonic devices without extra etching step to transfer patterns. Several groups have demonstrated the patterning of ChG large-core waveguides,[38-41] diffraction gratings [42-44] and wire-grid polarizers;[45] however, imprint fabrication of single-mode, sub-micron HIC devices (e.g. waveguides and resonators) has not been demonstrated. In addition, while resist pre-form reflow was previously adopted to produce microlenses and multi-level structures, [46-48] here we present the first effort to exploit the method's unique ability to produce a smooth surface finish required for low-loss photonic device processing.

2. EXPERIMENTAL SECTION

Bulk $As_{20}Se_{80}$ glasses were prepared using a traditional melt-quenching technique [25]. From the bulk glass target material, 360 nm-thick thin films were deposited by thermal evaporation. Thermal evaporation of powdered glass was carried out at a base pressure of $< 10^{-6}$ Torr in a single-source evaporator (PVD Products, Inc.). The deposition substrates are 3" silicon wafers coating with 3 μm thick thermal SiO_2. The deposition rate was maintained at ~ 16 Å/s. The substrate upon which the film was deposited was maintained at room temperature throughout the deposition. Thermal evaporation deposition conditions were optimized with respect to the optical performance of the deposited films (e.g. thickness uniformity and surface quality) and were highly repeatable. The substrates used for thin film deposition include 6" Si wafers with 3 μm thermal oxide (Silicon Quest International Inc.), epoxy-based (SU-8) polymer coated soda-lime

glass slides, 40 μm-thick Polyimide film (DuPont Inc.), and 80 μm-thick PET films (GoodFellow Inc.). More details concerning the bulk glass preparation and film deposition process may be found elsewhere. [49, 50]

An NR9-1000PY photoresist (Futurrex inc.) pattern was first defined on a Si wafer using contact photolithography on an Karl Suss MJB-3 mask aligner, and then a thermal treatment at 135 °C for 5 s was implemented to reflow the NR9 polymer resist and create a smooth surface finish. This photoresist pattern was used as the master mold which can be conveniently used many times (> 20 times in our experiments) as the template to produce polydimethylsiloxane (PDMS) soft stamps. 5 mm thick elastomer stamps were made by casting liquid PDMS (Sylgard 184, Dow Corning Inc., 5:1 mixing ratio between the monomer and the curing agent) onto the master mold, first baked at 80 °C for 12 hours and then baked at 110 °C for 5 hours to ensure that the PDMS was fully cured.

Imprint was performed in a glove box purged by N_2 to protect the chalcogenide glass films from oxidation. The glass film sample along with the soft stamp was placed on a hotplate pre-set at imprint temperature. Imprint pressure of approximately 0.13 MPa was applied by loading a metal block on the film-stamp assembly. After imprint, the hotplate was allowed to cool to below 60 °C at a ramp-down rate of 5 °C/min, before the sample was removed from the hotplate. The stamp was then manually delaminated from the glass film. Free-standing flexible photonic devices on epoxy-based polymer membranes were obtained by removing the soda-lime glass substrate in HF solutions.

The surface morphology and roughness was measured using tapping mode atomic force microscopy (AFM) on a Dimension 3100 (Digital Instruments, Inc.) microscope. To accurately measure the waveguide line edge roughness, AFM line scans were performed parallel to the waveguides to avoid line-to-line variations in a 2-D AFM scan. The scans were performed at 5 or more different locations on each sample and the results were averaged. Silicon AFM probes (Tap 150-G from Budget Sensors, Inc) with a force constant of 5 N/m and a resonant frequency of 150 KHz were used. The cross sectional images of imprinted waveguides/resonators were taken on a JSM-7400F (JEOL, Inc.) scanning electron microscope (SEM).

Before optical measurements, a 3 μm-thick SU-8 polymer (MicroChem Inc.) layer was spin coated on the patterned glass samples, which served as a top cladding and also prevented the glass films from oxidation. The waveguide facets on flexible substrates were prepared using focused Ga^{2+} ion beam milling (beam current 4 nA, accelerating voltage 30 kV) using a Zeiss Auriga 60 CrossBeam™ FIB nanoprototyping workstation. The transmission spectra of the micro-ring resonators were measured using a tunable laser (Agilent Technologies Model 81682A) operating in a step sweep mode. We used a fiber end-fire coupling method for coupling light into and out of the devices. All the measurement results reported in this paper use TE-polarized light.

3. RESULTS AND DISCUSSION

3.1 Nanoimprint process flow

In Figure 1, we depict the process flow to pattern HIC ChG photonic devices by nanoimprint. Photoresist line patterns were first defined on a pristine silicon substrate followed by thermal reflow of the photoresist lines to smooth their sidewalls. The surface cleanliness of Si wafers used in the process is crucial, as any contaminants can result in pinning of the resist line edges [51]. A PDMS elastomer stamp was subsequently replica molded from the resist line patterns. High-quality ChG films were deposited using vacuum thermal evaporation and subsequently imprinted following protocols outlined in the preceding section. In the last fabrication step, a 4 μm-thick SU-8 epoxy layer was spin coated on top of the patterned devices to serve as a top cladding to protect the devices from surface oxidation.

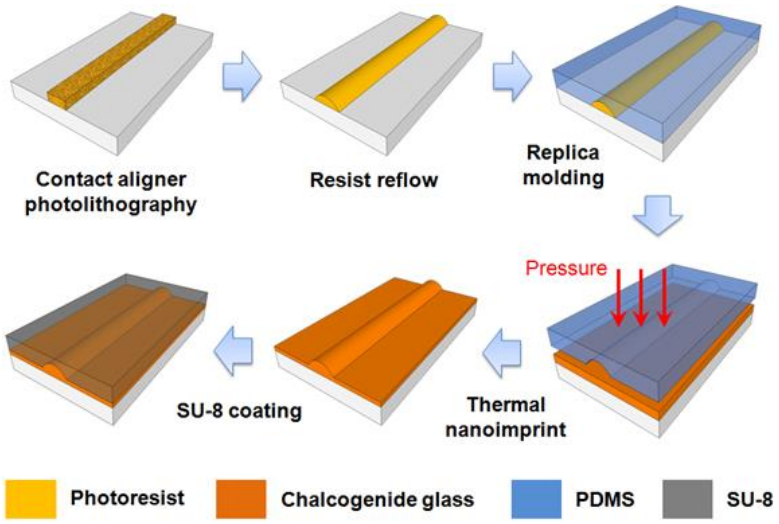

Figure 1. Schematic illustration of the thermal nanoimprint fabrication process

3.2 Optical Characterizations of Imprinted Devices

The optimal temperature and time for imprinting thermally evaporated $As_{20}Se_{80}$ films are set at 153 °C for 15 minutes, optimized based on SEM observations of imprinted device morphology and optical loss measurements. Figure 2 a and b are optical microscope images showing pulley-coupled micro-rings resonators imprinted on thermally evaporated $As_{20}Se_{80}$ films deposited on silicon wafers with 3 µm thermal oxide. Instead of using a simple “groove” on the PDMS stamp to define a ridge waveguide structure, we imprinted a pair of isolation trenches on both sides of the waveguide core, designed to displace the minimal amount of glass possible. The "minimum fluid displacement" strategy pioneered by Han *et al.* had been successfully applied to both polymer and glass imprints.[38, 41, 52] The morphology of the coupling region between the bus waveguide and the micro-ring has been characterized by AFM (Figure 2 c) confirming excellent pattern fidelity and a smooth surface finish.

Figure 2 d plots a typical measured TE-polarization transmission spectrum of a ring resonator imprinted in thermally evaporated $As_{20}Se_{80}$ films. By systematically varying the gap width between the bus waveguide and the micro-ring, the resonator was designed to operate in the over coupling regime near 1550 nm wavelength. Cavity quality factors (Q), defined as the ratio of wavelength against the resonant peak full width at half maximum, were measured by averaging over multiple devices. The measurement yielded an average loaded Q-factor of 100,000 in imprinted $As_{20}Se_{80}$ devices. A maximum loaded Q-factor of 150,000 was observed (Figure 2 e). Such a high Q-factor corresponds to an equivalent waveguide loss of 1.6 dB/cm and an intrinsic Q-factor of 390,000, the highest value reported in ChG micro-ring resonators. It is worth noting that our present result was obtained on devices patterned using a simple contact aligner, yet the Q value represents a 20-fold improvement over the Q's of our previously demonstrated ChG micro-ring resonators fabricated on an i-line stepper [53].

Optical loss in a micro-ring resonator can be attributed to several mechanisms. Specifically, the total loss is written as:

$$\alpha_{tot} = \alpha_{abs} + \alpha_{sca} + \alpha_{bend} + \alpha_{sub} \quad (1)$$

where α_{abs}, α_{sca}, α_{bend}, and α_{sub} denote optical losses associated with material absorption, surface and sidewall roughness scattering, waveguide bending, and substrate leakage, respectively. To assess the loss mechanisms in the imprinted micro-ring devices, we performed finite difference modal simulations using a full-vectorial bending mode solver incorporating cylindrical perfectly matching boundary layers (CPML) [54]. The model used waveguide dimensions experimentally measured from cross-sectional SEM images. According to the simulation results, substrate leakage loss is negligible and radiative leakage due to waveguide bending causes 0.1 dB/cm loss in our micro-ring device. The roughness scattering loss was estimated using the Payne-Lacey theory and surface roughness measured by AFM to be < 0.1 dB/cm [55]. Therefore, we conclude that material attenuation due to the $As_{20}Se_{80}$ glass accounts for approximately 1.5 dB/cm optical loss. The material loss, possibly resulting from nanoscale phase separation in ChGs as was observed in

[38], can be mitigated through decreasing the thermal treatment time by applying higher pressure during imprint. Therefore, we expect that our single-step imprint fabrication technique will likely lead to HIC single-mode photonic devices with optical loss well below 1 dB/cm.

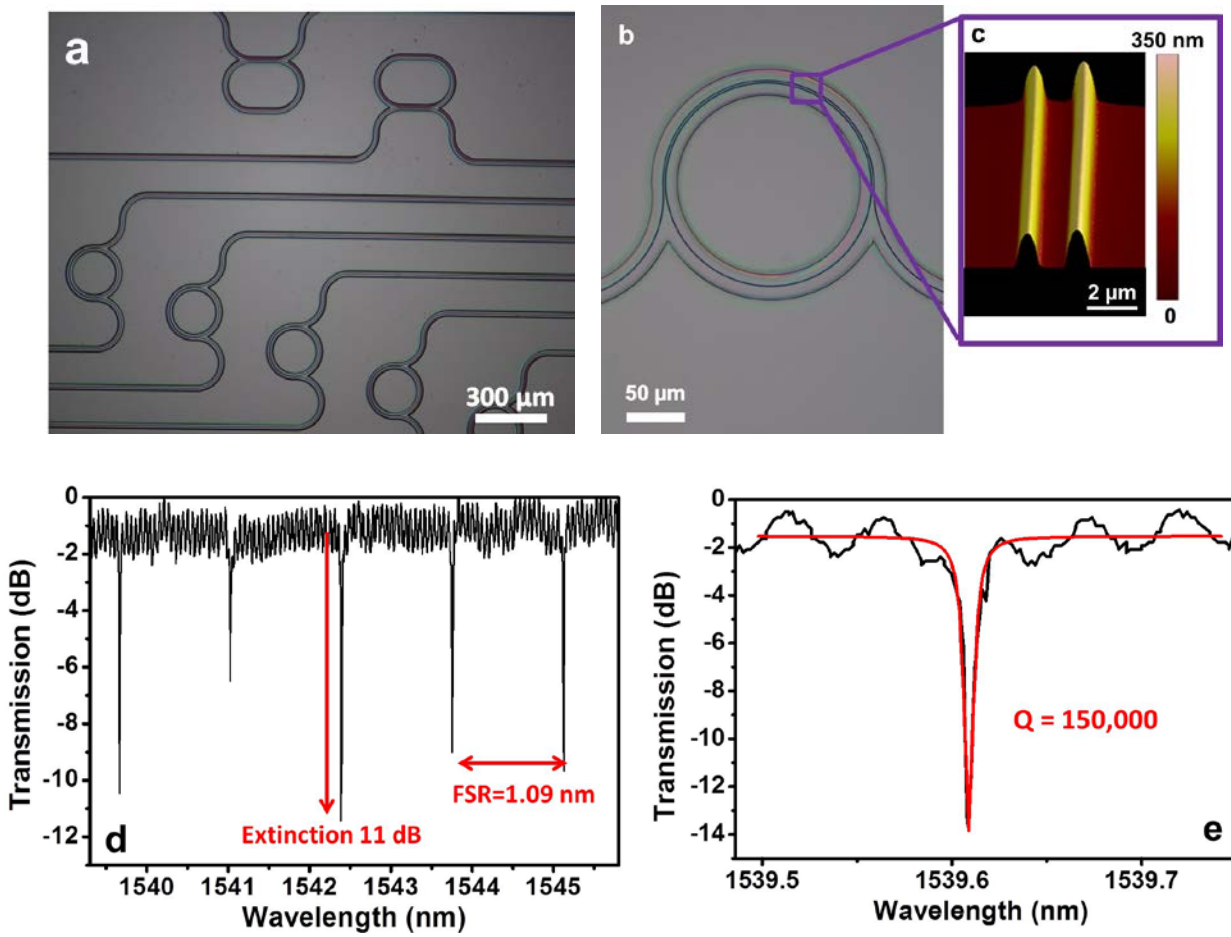

Figure 2. Optical Characterizations of Imprinted Devices. (a) and (b) Top-view microscopes image of imprinted $As_{20}Se_{80}$ micro-ring resonators with a radius of 100 µm; (c) surface morphology of a coupling section between a bus waveguide and a micro-ring measured by AFM, showing an RMS surface roughness of 0.8 nm. The coupling gap width is 800 nm; (d) TE-polarization transmission spectrum of an imprinted micro-ring resonator with an FSR of 1.09 nm; (e) transmission spectrum of a resonance peak showing an intrinsic Q-factor of 390,000, corresponding to an equivalent waveguide loss of 1.6 dB/cm

3.3 Direct Monolithic Imprint Fabrication on Nonplanar Substrates

We further demonstrated that the nanoimprint method is also applicable to HIC photonic integration on soft polymer substrates, for example epoxy-based SU-8 polymer, polyimide and polyethylene terephthalate (PET) plastic substrates, given the amorphous nature and low deposition temperature of ChG films. Figure 3 a is a macroscopic view of the imprinted $As_{20}Se_{80}$ glass devices on a 40 µm thick polyamide film, Figure 3 b shows an optical microscope image of the devices, and Figure 3 c plots the measured transmission spectrum of a flexible micro-ring resonator patterned on a free-standing SU-8 membrane. The flexible resonators exhibited an average intrinsic Q value of 110,000. The number is slightly lower compared to devices printed on Si substrates but is 50 times higher than previous reports of monolithically integrated optical resonator structures on flexible substrates [56]. The lower Q is likely due to the inferior surface quality of the flexible substrate. Compared to the standard transfer printing protocols for device fabrication on flexible substrates, the direct imprint patterning approach offers a monolithic integration alternative with potentially improved throughput and yield, and may also enables roll-to-roll processing of HIC photonic devices over large substrate areas inaccessible using conventional lithographic patterning methods.

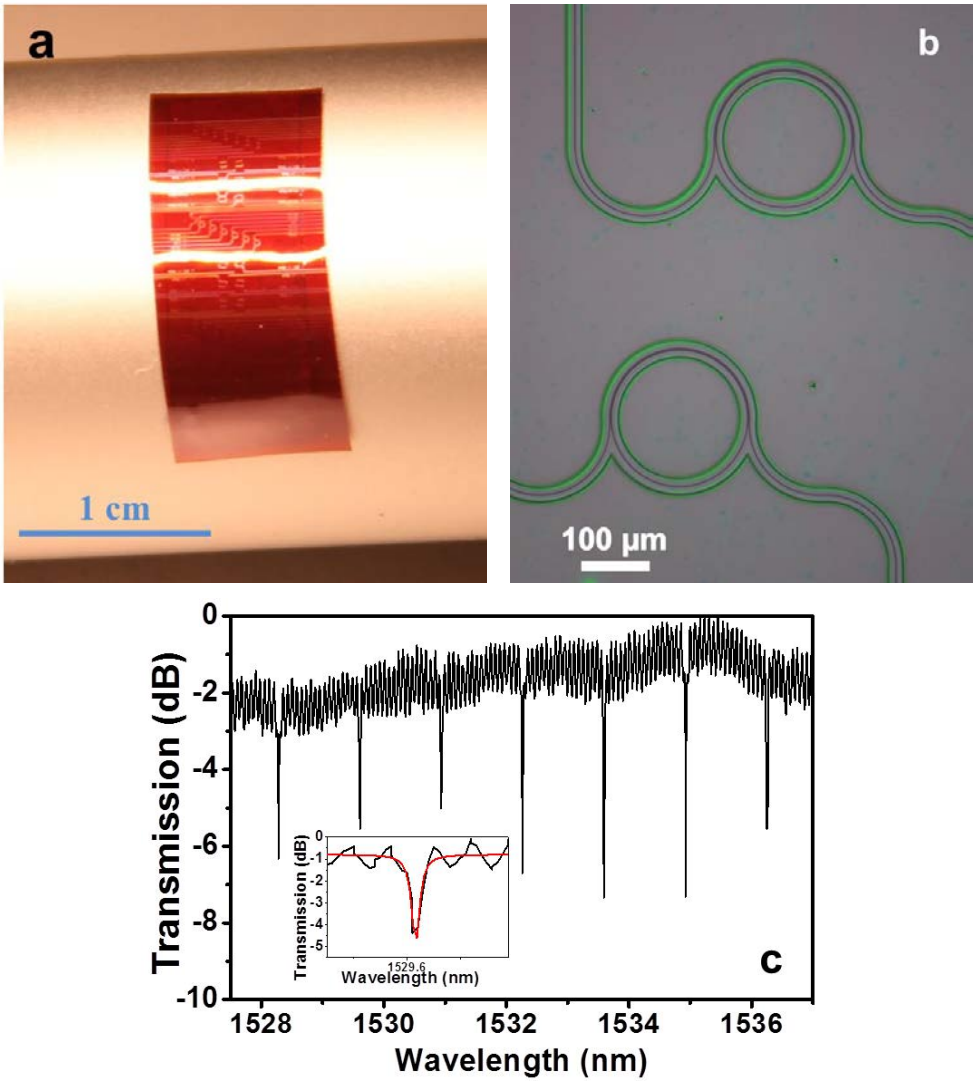

Figure 3. Direct Monolithic Imprint Fabrication on Nonplanar Substrates. (a) A photo showing imprinted ChG resonator devices on a flexible polyamide substrate; (b) top-view microscope image of ChG ring resonators imprinted on a flexible polyimide film; (c) transmission spectrum of an imprinted $As_{20}Se_{80}$ micro-ring resonator on a flexible substrate: an average intrinsic Q = 110,000 was measured on the spectrum shown in the inset.

4. CONCLUSION

To conclude, we report a simple, substrate-blind direct nanoimprint approach for high-performance, high-index-contrast glass photonic device fabrication. The method combines resist reflow and thermal nanoimprint to achieve an ultra-smooth surface finish on fabricated devices and hence low optical loss. We used the technique to demonstrate ChG micro-ring resonators with a record intrinsic Q-factor of 390,000 at 1550 nm wavelength. Furthermore, the low processing temperature of our technique is fully compatible with photonic integration on flexible polymer substrates, and we successfully applied the method to monolithically fabricate HIC glass photonic devices on plastic substrates. The technique is also compatible with CMOS backend integration given its minimal thermal budget requirement, making it potentially attractive for an array of emerging applications ranging from optical interconnects to conformal photonic sensor integration on complex curvilinear surfaces.

5. ACKNOWLEDGEMENTS

The authors would like to thank funding support provided by the Department of Energy under award number DE-EE0005327 and the University of Delaware Research Foundation (UDRF). UCF co-authors acknowledge funding provided in part by the US Department of Energy [Contract # DE- NA000421], NNSA/DNN R&D.

REFERENCES

[1] Barrios, C. A., and Lipson, M., "Electrically driven silicon resonant light emitting device based on slot-waveguide," Opt. Express, 13(25), 10092-10101 (2005).
[2] Xu, Q. F., Almeida, V. R., and Lipson, M., "Demonstration of high Raman gain in a submicrometer-size silicon-on-insulator waveguide," Opt. Lett., 30(1), 35-37 (2005).
[3] Hu, J. J., Carlie, N., Feng, N. N., Petit, L., Agarwal, A., Richardson, K., and Kimerling, L., "Planar waveguide-coupled, high-index-contrast, high-Q resonators in chalcogenide glass for sensing," Opt. Lett., 33(21), 2500-2502 (2008).
[4] Barwicz, T., and Haus, H. A., "Three-dimensional analysis of scattering losses due to sidewall roughness, in microphotonic waveguides," J. Lightwave Technol., 23(9), 2719-2732 (2005).
[5] Barwicz, T., and Smith, H. I., "Evolution of line-edge roughness during fabrication of high-index-contrast microphotonic devices," J. Vac. Sci. Technol. B, 21(6), 2892-2896 (2003).
[6] Sparacin, D. K., Spector, S. J., and Kimerling, L. C., "Silicon waveguide sidewall smoothing by wet chemical oxidation," J. Lightwave Technol., 23(8), 2455-2461 (2005).
[7] Lee, K. K., Lim, D. R., Kimerling, L. C., Shin, J., and Cerrina, F., "Fabrication of ultralow-loss Si/SiO2 waveguides by roughness reduction," Opt. Lett., 26(23), 1888-1890 (2001).
[8] Lee, M. C. M., and Wu, M. C., "Thermal annealing in hydrogen for 3-D profile transformation on silicon-on-insulator and sidewall roughness reduction," J. Microelectromech. Syst., 15(2), 338-343 (2006).
[9] Hung, S. C., Liang, E. Z., and Lin, C. F., "Silicon Waveguide Sidewall Smoothing by KrF Excimer Laser Reformation," J. Lightwave Technol., 27(5-8), 887-892 (2009).
[10] Chao, C. Y., and Guo, L. J., "Reduction of surface scattering loss in polymer microrings using thermal-reflow technique," IEEE Photonics Technol. Lett., 16(6), 1498-1500 (2004).
[11] Hu, J. J., Feng, N. N., Carlie, N., Petit, L., Agarwal, A., Richardson, K., and Kimerling, L., "Optical loss reduction in high-index-contrast chalcogenide glass waveguides via thermal reflow," Opt. Express, 18(2), 1469-1478 (2010).
[12] Chou, S. Y., Krauss, P. R., and Renstrom, P. J., "Imprint lithography with 25-nanometer resolution," Science, 272(5258), 85-87 (1996).
[13] Suh, K. Y., Kim, Y. S., and Lee, H. H., "Capillary force lithography," Adv. Mater., 13(18), 1386-1389 (2001).
[14] Xia, Y. N., and Whitesides, G. M., "Soft lithography," Angew. Chem.-Int. Edit., 37(5), 551-575 (1998).
[15] Ahn, S. H., and Guo, L. J., "High-speed roll-to-roll nanoimprint lithography on flexible plastic substrates," Adv. Mater., 20(11), 2044-+ (2008).
[16] Ahn, S. H., and Guo, L. J., "Large-Area Roll-to-Roll and Roll-to-Plate Nanoimprint Lithography: A Step toward High-Throughput Application of Continuous Nanoimprinting," ACS Nano, 3(8), 2304-2310 (2009).
[17] Stuart, C., and Chen, Y., "Roll in and Roll out: A Path to High-Throughput Nanoimprint Lithography," ACS Nano, 3(8), 2062-2064 (2009).
[18] Guo, L. J., "Nanoimprint lithography: Methods and material requirements," Adv. Mater., 19(4), 495-513 (2007).
[19] Chang, C. H., Montoya, J. C., Akilian, M., Lapsa, A., Heilmann, R. K., Schattenburg, M. L., Li, M., Flanagan, K. A., Rasmussen, A. P., Seely, J. F., Laming, J. M., Kjornrattanawanich, B., and Goray, L. I., "High fidelity blazed grating replication using nanoimprint lithography," J. Vac. Sci. Technol. B, 22(6), 3260-3264 (2004).
[20] Chao, C. Y., and Guo, L. J., "Polymer microring resonators fabricated by nanoimprint technique," J. Vac. Sci. Technol. B, 20(6), 2862-2866 (2002).
[21] Huang, Y. Y., Paloczi, G. T., Yariv, A., Zhang, C., and Dalton, L. R., "Fabrication and replication of polymer integrated optical devices using electron-beam lithography and soft lithography," J. Phys. Chem. B, 108(25), 8606-8613 (2004).

[22] Ji, R., Hornung, M., Verschuuren, M. A., van de Laar, R., van Eekelen, J., Plachetka, U., Moeller, M., and Moormann, C., "UV enhanced substrate conformal imprint lithography (UV-SCIL) technique for photonic crystals patterning in LED manufacturing," Microelectron. Eng., 87(5-8), 963-967 (2010).
[23] Teng, J., Scheerlinck, S., Zhang, H. B., Jian, X. G., Morthier, G., Beats, R., Han, X. Y., and Zhao, M. S., "A PSQ-L Polymer Microring Resonator Fabricated by a Simple UV-Based Soft-Lithography Process," IEEE Photonics Technol. Lett., 21(18), 1323-1325 (2009).
[24] Ting, C. J., Huang, M. C., Tsai, H. Y., Chou, C. P., and Fu, C. C., "Low cost fabrication of the large-area anti-reflection films from polymer by nanoimprint/hot-embossing technology," Nanotechnology, 19(20), (2008).
[25] Musgraves, J. D., Wachtel, P., Novak, S., Wilkinson, J., and Richardson, K., "Composition dependence of the viscosity and other physical properties in the arsenic selenide glass system," J. Appl. Phys., 110(6), (2011).
[26] Sanghera, J. S., and Aggarwal, I. D., "Active and passive chalcogenide glass optical fibers for IR applications: a review," J. Non-Cryst. Solids, 257, 6-16 (1999).
[27] Zakery, A., and Elliott, S. R., "Optical properties and applications of chalcogenide glasses: a review," J. Non-Cryst. Solids, 330(1-3), 1-12 (2003).
[28] Asobe, M., "Nonlinear optical properties of chalcogenide glass fibers and their application to all-optical switching," Opt. Fiber Technol., 3(2), 142-148 (1997).
[29] Tanaka, K., "Optical nonlinearity in photonic glasses," J. Mater. Sci.-Mater. Electron., 16(10), 633-643 (2005).
[30] Eggleton, B. J., Luther-Davies, B., and Richardson, K., "Chalcogenide photonics," Nat. Photonics, 5(3), 141-148 (2011).
[31] Zou, Y., Lin, H. T., Ogbuu, O., Li, L., Danto, S., Novak, S., Novak, J., Musgraves, J. D., Richardson, K., and Hu, J. J., "Effect of annealing conditions on the physio-chemical properties of spin-coated As2Se3 chalcogenide glass films," Opt. Mater. Express, 2(12), 1723-1732 (2012).
[32] Lucas, P., "Energy landscape and photoinduced structural changes in chalcogenide glasses," J. Phys.-Condes. Matter, 18(24), 5629-5638 (2006).
[33] Petit, L., Carlie, N., Anderson, T., Choi, J., Richardson, M., and Richardson, K. C., "Progress on the Photoresponse of Chalcogenide Glasses and Films to Near-Infrared Femtosecond Laser Irradiation: A Review," IEEE J. Sel. Top. Quantum Electron., 14(5), 1323-1334 (2008).
[34] Hu, J. J., "Ultra-sensitive chemical vapor detection using micro-cavity photothermal spectroscopy," Opt. Express, 18(21), 22174-22186 (2010).
[35] Lin, H. T., Yi, Z., and Hu, J. J., "Double resonance 1-D photonic crystal cavities for single-molecule mid-infrared photothermal spectroscopy: theory and design," Opt. Lett., 37(8), 1304-1306 (2012).
[36] DeCorby, R. G., Ponnampalam, N., Nguyen, H. T., and Clement, T. J., "Robust and flexible free-standing all-dielectric omnidirectional reflectors," Adv. Mater., 19(2), 193-+ (2007).
[37] Dmitriev, S. V., and Dementiev, I. V., [Vitreous chalcogenide semiconductors for gas sensing application], (2005).
[38] Han, T., Madden, S., Bulla, D., and Luther-Davies, B., "Low loss Chalcogenide glass waveguides by thermal nano-imprint lithography," Opt. Express, 18(18), 19286-19291 (2010).
[39] Lian, Z. G., Pan, W. J., Furniss, D., Benson, T. M., Seddon, A. B., Kohoutek, T., Orava, J., and Wagner, T., "Embossing of chalcogenide glasses: monomode rib optical waveguides in evaporated thin films," Opt. Lett., 34(8), 1234-1236 (2009).
[40] Pan, W. J., Rowe, H., Zhang, D., Zhang, Y., Loni, A., Furniss, D., Sewell, P., Benson, T. M., and Seddon, A. B., "One step hot embossing of optical rib waveguides in chalcogenide glasses," Microw. Opt. Technol. Lett., 50(7), 1961-1963 (2008).
[41] Han, T., Madden, S., Debbarma, S., and Luther-Davies, B., "Improved method for hot embossing As2S3 waveguides employing a thermally stable chalcogenide coating," Opt. Express, 19(25), 25447-25453 (2011).
[42] Orava, J., Kohoutek, T., Greer, A. L., and Fudouzi, H., "Soft imprint lithography of a bulk chalcogenide glass," Opt. Mater. Express, 1(5), 796-802 (2011).
[43] Silvennoinen, M., Paivasaari, K., Kaakkunen, J. J. J., Tikhomirov, V. K., Lehmuskero, A., Vahimaa, P., and Moshchalkov, V. V., "Imprinting the nanostructures on the high refractive index semiconductor glass," Appl. Surf. Sci., 257(15), 6829-6832 (2011).
[44] Solmaz, M., Park, H., Madsen, C. K., and Cheng, X., "Patterning chalcogenide glass by direct resist-free thermal nanoimprint," J. Vac. Sci. Technol. B, 26(2), 606-610 (2008).
[45] Yamada, I., Yamashita, N., Tani, K., Einishi, T., Saito, M., Fukumi, K., and Nishii, J., "Fabrication of a mid-IR wire-grid polarizer by direct imprinting on chalcogenide glass," Opt. Lett., 36(19), 3882-3884 (2011).

[46] Peng, C., Liang, X. G., Fu, Z. L., and Chou, S. Y., "High fidelity fabrication of microlens arrays by nanoimprint using conformal mold duplication and low-pressure liquid material curing," J. Vac. Sci. Technol. B, 25(2), 410-414 (2007).
[47] Schleunitz, A., and Schift, H., "Fabrication of 3D nanoimprint stamps with continuous reliefs using dose-modulated electron beam lithography and thermal reflow," J. Micromech. Microeng., 20(9), (2010).
[48] Schift, H., Spreu, C., Schleunitz, A., and Lee, J., "Shape control of polymer reflow structures fabricated by nanoimprint lithography," Microelectron. Eng., 88(1), 87-92 (2011).
[49] Petit, L., Carlie, N., Adamietz, F., Couzi, M., Rodriguez, V., and Richardson, K. C., "Correlation between physical, optical and structural properties of sulfide glasses in the system Ge-Sb-S," Mater. Chem. Phys., 97(1), 64-70 (2006).
[50] Hu, J. J., Tarasov, V., Agarwal, A., Kimerling, L., Carlie, N., Petit, L., and Richardson, K., "Fabrication and testing of planar chalcogenide waveguide integrated microfluidic sensor," Opt. Express, 15(5), 2307-2314 (2007).
[51] Tsay, C., Zha, Y. L., and Arnold, C. B., "Solution-processed chalcogenide glass for integrated single-mode mid-infrared waveguides," Opt. Express, 18(25), 26744-26753 (2010).
[52] Han, T., Madden, S., Zhang, M., Charters, R., and Luther-Davies, B., "Low loss high index contrast nanoimprinted polysiloxane waveguides," Opt. Express, 17(4), 2623-2630 (2009).
[53] Hu, J. J., Carlie, N., Petit, L., Agarwal, A., Richardson, K., and Kimerling, L., "Demonstration of chalcogenide glass racetrack microresonators," Opt. Lett., 33(8), 761-763 (2008).
[54] Feng, N. N., Zhou, G. R., Xu, C. L., and Huang, W. P., "Computation of full-vector modes for bending waveguide using cylindrical perfectly matched layers," J. Lightwave Technol., 20(11), 1976-1980 (2002).
[55] Lacey, J. P. R., and Payne, F. P., "Radiation loss from planar waveguides with random wall imperfections," IEE Proc. J., 137(4), 282-288 (1990).
[56] Fan, L., Varghese, L. T., Xuan, Y., Wang, J., Niu, B., and Qi, M. H., "Direct fabrication of silicon photonic devices on a flexible platform and its application for strain sensing," Opt. Express, 20(18), 20564-20575 (2012).